

Primal HDG Methods for Elliptic Problems on Curved Meshes

Ismael de Souza Ledoino¹, Abimael Fernando Dourado Loula¹

¹Laboratório Nacional de Computação Científica - LNCC
Av. Getúlio Vargas, 333, 25651-075, Rio de Janeiro/RJ, Brazil
iledoino@lncc.br; aloc@lncc.br

Abstract. This work addresses stability and locking of three classes of hybrid methods for elliptic problems on straight and curved meshes in $2d$. We consider here modifications of the hybrid methods presented in [1] and [2], and compare them with the hybrid high order method discussed in [3]. For straight meshes, the approximation order for polynomial spaces over edges can either be equal or one order smaller than the approximation order for polynomial spaces in the interior. However, having one order smaller for edges is actually mandatory for obtaining locking-free estimates from our modification of the primal method introduced in [1] on straight meshes (except for triangles, where the approximation spaces are divergence-free). The other two hybrid methods are locking-free whenever they are stable. In the case of curved meshes, we verify that all three methods are unstable if one chooses approximation orders for the edges one order smaller than the interior. However, we also verify numerically that all three methods are locking-free in curved meshes if these polynomial orders are equal.

Keywords: HDG Methods, Reduced Integration, Curved Meshes, Linear Elasticity, Locking-Free

1 Introduction

Many different finite element techniques have been applied to solve the linear elasticity problem in the past decades [1, 4–8]. The classical approach is based on formulations that provide approximations to the displacement field, being the stress field recovered through post-processing [9]. Such formulations have the disadvantage that the stress is usually recovered with poor accuracy using standard post-processing techniques (direct derivation of displacement). Since stress is usually the main variable of interest, mixed formulations have been developed to provide guaranteed optimal rates of convergence for both the displacement and stress fields [8, 10–12]. The spaces developed in [12] were showed to provide good results even in the nearly incompressible regime. Discontinuous Galerkin methods have also been applied successfully to this class of problems [13–16], mostly due to their robustness and flexibility for implementing h and p adaptivity techniques. Hybrid DG formulations keep these properties adding to the list the advantage of less degrees of freedom for higher order spaces, since static condensation can be naturally used to obtain a linear system with only Lagrange multiplier degrees of freedom, see [1].

Among the advantages of HDG over DG methods are the less complicated assembly, natural hp -adaptivity, and reduction of degrees of freedom in the global linear system by static condensation. All of these benefits are acquired mostly due to the presence of Lagrange multipliers, which in addition increase stability because of the weak satisfaction of the jump conditions over element interfaces. The very own presence of Lagrange multipliers can have undesired consequences, however. For instance, both DG and HDG methods can use physical-frame polynomials rather than reference-frame ones, since no strong continuity of the basis functions over element interfaces is required. However, on curved meshes, using reference-frame polynomials over interfaces seems a natural choice. On the other hand, DG methods promptly apply to curved meshes, with the only difference to straight meshes being that numerically calculating the integrals may require more integration points. Another point in favor of DG methods for our model problem, specifically those presented in [15], is that their symmetric version is locking-free without any need of projections in the boundary terms. We verify in this work that this does not happen to their HDG counterparts: the projection operators are essential for a locking-free estimate of the displacements. Although using these projections may require more computations for $d = 3$, doing so along with static condensation also generates a smaller linear global system, which more than outperforms the extra computation needed for boundary integrals, in general. In addition, using reduced integration on the boundary terms has the same effect of using projection operators in $d = 2$, which makes using projections even less expensive

than otherwise.

In the sections to come, we start by introducing notation and polynomial spaces used in the hybrid methods. We proceed by a resumed presentation of modified formulations from [1] and [2], which differ from the original works in the presence of projection operators in the boundary terms. In the section that follows, we briefly discuss the impact of curved meshes on hybrid methods, emphasizing the a priori requirement on the polynomial order of Lagrange multipliers in this case. Finally, we present numerical results that verify stability and locking-free property of the hybrid methods discussed.

2 Preliminaries

Let $H^m(\Omega)$ denote the usual Sobolev space equipped with the norm $\|\cdot\|_{m,\Omega} = \|\cdot\|_m$ and the associated seminorm $|\cdot|_{m,\Omega} = |\cdot|_m$, with $m \geq 0$. For $m = 0$, we set $L^2(\Omega) = H^0(\Omega)$ as the space of square integrable functions and $H_0^1(\Omega)$ the subspace of functions in $H^1(\Omega)$ with zero trace on $\partial\Omega$. In addition, we set $L_0^2(\Omega) = \{q \in L^2(\Omega) : \int_{\Omega} q \, d\mathbf{x} = 0\}$ to be the space of square integrable functions that have zero average in Ω . For vector-valued functions, we use bold symbols to refer to the corresponding vector spaces: $\mathbf{H}^m := [H^m]^d$, $\mathbf{H}_0^m := [H_0^m]^d$, $\mathbf{L}^2 := [L^2]^d$ and $\mathbf{L}_0^2 := [L_0^2]^d$.

We define $\{\mathcal{T}_h\}_h$ to be a family of meshes of $\Omega \subset \mathbb{R}^d$ into disjoint open polytopal elements K , star-shaped with respect to a ball of radius ρ_K . The union of the closures of the elements $K \in \mathcal{T}_h$ forms a covering of the closure of Ω , i.e., $\bar{\Omega} = \cup_{K \in \mathcal{T}_h} \bar{K}$. The interfaces of the computational mesh \mathcal{T}_h are united in $\mathcal{E}_h = \{e; e \text{ is a facet of } K \text{ for all } K \in \mathcal{T}_h\}$, the interior facets are contained in $\mathcal{E}_h^0 = \{e; e \in \mathcal{E}_h; e \text{ is the interior facet}\}$, and the boundary ones belong to $\mathcal{E}_h^\partial = \{e; e \in \mathcal{E}_h; e \subset \partial\Omega\}$. We assume that the domain Ω is polytopal and \mathcal{T}_h is a regular partition of Ω . Thus, there exists $\gamma_e > 0$ such that $h_K \leq \gamma_e h_e$, where $h_e := \text{diam}(e)$ is the diameter of the facet $e \in \partial K$. We also assume that the facets in \mathcal{E}_h do not degenerate with refinement. For each element K we associate a unit outward normal vector \mathbf{n}_K , and when there is not a chance for confusion, we write simply \mathbf{n} .

We will use \mathcal{V}_h^k and \mathcal{Q}_h^l to denote the broken finite dimensional spaces on the partition \mathcal{T}_h , defined as:

$$\mathcal{V}_h^k = \{\mathbf{v} \in \mathbf{L}^2(\Omega); \mathbf{v}|_K \in [\mathbb{P}_k^d(K)]^d, \forall K \in \mathcal{T}_h\}; \quad \mathcal{Q}_h^l = \{q \in L^2(\Omega); q|_K \in \mathbb{P}_l^d(K), \forall K \in \mathcal{T}_h\}, \quad (1)$$

with $\mathbb{P}_k^d(K)$ being the d -dimensional space of polynomial functions of degree at most k on K . The Lagrange multiplier associated with the trace of the displacement field $\hat{\mathbf{u}} = \mathbf{u}|_e$ on each facet $e \in \mathcal{E}_h$ is chosen to live at

$$\mathcal{M}_h^m = \{\hat{\mathbf{v}}_h \in \mathbf{L}^2(\mathcal{E}_h) : \hat{\mathbf{v}}_h|_e \in [\mathbb{P}_m^{d-1}(\sigma) \circ \Psi_e^{-1}]^d, e = \Psi_e(\sigma), \forall e \in \mathcal{E}_h^0; \hat{\mathbf{v}}_h|_e = \bar{\mathbf{u}}_h, \forall e \in \mathcal{E}_h^\partial\}, \quad (2)$$

$$\bar{\mathcal{M}}_h^m = \{\hat{\mathbf{v}}_h \in \mathbf{L}^2(\mathcal{E}_h) : \hat{\mathbf{v}}_h|_e \in [\mathbb{P}_m^{d-1}(\sigma) \circ \Psi_e^{-1}]^d, e = \Psi_e(\sigma), \forall e \in \mathcal{E}_h^0; \hat{\mathbf{v}}_h|_e = \mathbf{0}, \forall e \in \mathcal{E}_h^\partial\}, \quad (3)$$

with $\mathbb{P}_m^{d-1}(\sigma)$ denoting the $(d-1)$ -dimensional space of polynomial functions of degree at most m on the reference facet σ , mapped to the physical facet e by the mapping Ψ_e . In the space \mathcal{M}_h^m above, $\bar{\mathbf{u}}_h$ is the local $L^2(e)$ projection of the Dirichlet boundary condition function $\bar{\mathbf{u}}$ on each $e \in \mathcal{E}_h^\partial$ in (2). These numerical spaces are all defined using approximation spaces \mathbb{P}_k^d on general polytopes, although we use here only triangles, quadrilaterals and randomly distorted 9-node quadrilaterals.

3 The Model Problem

As model problem we consider the linear and isotropic elasticity problem in its displacement formulation, governed by the differential equation

$$-\text{div } \boldsymbol{\sigma} = \mathbf{f}, \quad \text{with } \boldsymbol{\sigma}(\mathbf{u}) = \mathbb{D}\boldsymbol{\varepsilon}(\mathbf{u}) = 2\mu\boldsymbol{\varepsilon}(\mathbf{u}) + \lambda(\text{tr}\boldsymbol{\varepsilon}(\mathbf{u}))\mathbb{I}, \quad (4)$$

where $\mathbb{D} = 2\mu\mathbb{I} + \lambda\mathbb{I} \otimes \mathbb{I}$ is the isotropic elasticity tensor, $\boldsymbol{\varepsilon}(\mathbf{u}) = \frac{1}{2}(\nabla\mathbf{u} + \nabla\mathbf{u}^T)$ is the symmetric part of the gradient of \mathbf{u} (linear strain tensor), $\text{tr}\boldsymbol{\varepsilon}(\mathbf{u}) = \text{div } \mathbf{u}$ is the volumetric deformation, \mathbb{I} is the fourth-order identity tensor on symmetric second-order tensors, \mathbb{I} is the second-order identity tensor and λ and μ are the Lamé coefficients. For linear plane strain, the Lamé coefficients are given by $\lambda = E\nu/[(1+\nu)(1-2\nu)]$, and $\mu = E/[2(1+\nu)]$, where E is the elasticity modulus and ν is the Poisson's ratio. Equation (4) leads to a displacement-based problem as follows: find the displacement field $\mathbf{u} : \Omega \rightarrow \mathbb{R}^2$ such that

$$-\text{div } \mathbb{D}\boldsymbol{\varepsilon}(\mathbf{u}) = \mathbf{f}, \quad \text{in } \Omega, \quad (5)$$

with $\mathbf{u} = \mathbf{0}$, on $\partial\Omega$. Existence and uniqueness of solution to the problem above is proved in the infinite dimensional space $\mathbf{V}(\Omega) = \mathbf{H}_0^1(\Omega)$. The primal continuous Galerkin formulation for this problem has a numeric counterpart

that suffers from poor accuracy in the nearly incompressible regime ($\nu \rightarrow 1/2$). A way to circumvent this issue is by rewriting the equations in terms of the displacement field \mathbf{u} and a hydrostatic pressure ϕ , in which we define $\phi := -\lambda \operatorname{div} \mathbf{u}$. This mixed version of the problem consists of seeking the solution to equations in (5) by solving the equivalent problem: find the displacement field $\mathbf{u} : \Omega \rightarrow \mathbb{R}^2$ and the hydrostatic pressure $\phi : \Omega \rightarrow \mathbb{R}$, such that

$$\begin{cases} -2\mu \operatorname{div} \boldsymbol{\varepsilon}(\mathbf{u}) + \nabla \phi = \mathbf{f} & \text{in } \Omega, \\ -\frac{1}{\lambda} \phi - \operatorname{div} \mathbf{u} = 0 & \text{in } \Omega, \end{cases} \quad (6)$$

with $\mathbf{u} = \mathbf{0}$ on $\partial\Omega$. Existence and uniqueness of solution to the problem above is proved in the infinite dimensional space $\mathbf{V}(\Omega) \times Q(\Omega) = \mathbf{H}_0^1(\Omega) \times L_0^2(\Omega)$ by applying Babuška's Lemma [17], as shown in [2].

4 Finite Element Approximations

In this section we present the numerical methods discussed in the sections to come. We consider two stabilized primal hybrid methods based on problem (5), and a stabilized mixed hybrid method we have designed for equations in (6). The primal hybrid formulations were introduced in [1] and in [3], while the mixed hybrid formulation was analyzed in [2].

Stabilized Primal Hybrid Method: a stabilized primal hybrid (SPH) method for the differential form (5) of the linear elasticity problem was presented and analyzed in [1]. We propose here a slight variation of the formulation discussed in the reference: for each $K \in \mathcal{T}_h$, find $\mathbf{u}_h|_K \in \mathcal{V}_h^k(K)$, and for each $e \in \mathcal{E}_h^0$, find $\hat{\mathbf{u}}_h|_e \in \mathcal{M}_h^m$, such that

$$\mathbf{a}_{SPH}([\mathbf{u}_h, \hat{\mathbf{u}}_h], [\mathbf{v}_h, \hat{\mathbf{v}}_h]) = \mathbf{f}_{SPH}([\mathbf{v}_h, \hat{\mathbf{v}}_h]), \quad \text{with} \quad (7)$$

$$\begin{aligned} \mathbf{a}_{SPH}([\mathbf{u}_h, \hat{\mathbf{u}}_h], [\mathbf{v}_h, \hat{\mathbf{v}}_h]) &:= (\mathbb{D}\boldsymbol{\varepsilon}(\mathbf{u}_h), \boldsymbol{\varepsilon}(\mathbf{v}_h))_{\mathcal{T}_h} - \langle \mathbb{D}\boldsymbol{\varepsilon}(\mathbf{u}_h) \mathbf{n}_K, (\mathbf{v}_h - \hat{\mathbf{v}}_h) \rangle_{\partial\mathcal{T}_h} \\ &\quad + \theta \langle \mathbb{D}\boldsymbol{\varepsilon}(\mathbf{v}_h) \mathbf{n}_K, (\mathbf{u}_h - \hat{\mathbf{u}}_h) \rangle_{\partial\mathcal{T}_h} + \mathbf{s}_{SPH}([\mathbf{u}_h, \hat{\mathbf{u}}_h], [\mathbf{v}_h, \hat{\mathbf{v}}_h]), \\ \mathbf{f}_{SPH}([\mathbf{v}_h, \hat{\mathbf{v}}_h]) &:= (\mathbf{f}, \mathbf{v}_h)_{\mathcal{T}_h}, \end{aligned} \quad (8)$$

for all $\mathbf{v}_h \in \mathcal{V}_h^k(K)$ and for all $\hat{\mathbf{v}}_h \in \mathcal{M}_h^m$, where the symmetrization parameter θ may assume values $-1, 0$ or 1 . The stabilization bilinear form $\mathbf{s}_{SPH}(\cdot, \cdot)$ is given by

$$\begin{aligned} \mathbf{s}_{SPH}([\mathbf{u}_h, \hat{\mathbf{u}}_h], [\mathbf{v}_h, \hat{\mathbf{v}}_h]) &= 2\mu \frac{\beta_0}{h} \langle \pi_{\partial K}^m(\mathbf{u}_h - \hat{\mathbf{u}}_h), \pi_{\partial K}^m(\mathbf{v}_h - \hat{\mathbf{v}}_h) \rangle_{\partial\mathcal{T}_h} \\ &\quad + \lambda \frac{\beta_1}{h} \langle \pi_{\partial K}^m(\mathbf{u}_h - \hat{\mathbf{u}}_h) \cdot \mathbf{n}_K, \pi_{\partial K}^m(\mathbf{v}_h - \hat{\mathbf{v}}_h) \cdot \mathbf{n}_K \rangle_{\partial\mathcal{T}_h}, \end{aligned} \quad (9)$$

where $\pi_{\partial K}^m|_e = \pi_{\sigma}^m \circ \boldsymbol{\Psi}_e^{-1}$ is the $|J_{\boldsymbol{\Psi}_e}|^{1/2}$ -weighted L^2 orthogonal projector to the space $[\mathbb{P}_m^{d-1}(\sigma) \circ \boldsymbol{\Psi}_e^{-1}]^d$, for $J_{\boldsymbol{\Psi}_e}$ being the Jacobian of the mapping $\boldsymbol{\Psi}_e$, and $\beta_0, \beta_1 > 0$ are stabilization parameters that must be chosen large enough. This stabilization form differs from the original work [1] in the presence of the projection operator $\pi_{\partial K}^m$. This modification makes the formulation a locking-free method under some restrictions to m , which we discuss latter on in this work.

Stabilized Mixed Hybrid Method: a stabilized mixed hybrid method for our model problem, based on the Stokes-like formulation (6), has been proposed and analyzed in [2]. This method has been proven to be uniformly stable, and therefore locking-free, in every stable combination of the polynomial degrees k, l and m . The method can be written in the following form: for each $K \in \mathcal{T}_h$, find $\mathbf{u}_h|_K \in \mathcal{V}_h^k(K)$ and $\phi_h|_K \in \mathcal{Q}_h^l(K)$, and for each $e \in \mathcal{E}_h^0$, find $\hat{\mathbf{u}}_h \in \mathcal{M}_h^m$ such that

$$a_{SMH}^E([\mathbf{u}_h, \hat{\mathbf{u}}_h], [\mathbf{v}_h, \hat{\mathbf{v}}_h]) + b_{SMH}(\phi_h, [\mathbf{v}_h, \hat{\mathbf{v}}_h]) = f_{SMH}([\mathbf{v}_h, \hat{\mathbf{v}}_h]), \quad (10)$$

$$a_{SMH}^S(\phi_h, \varphi_h) + b_{SMH}(\varphi_h, [\mathbf{u}_h, \hat{\mathbf{u}}_h]) = 0, \quad (11)$$

for all $\mathbf{v}_h|_K \in \mathcal{V}_h^k(K)$, $\varphi_h|_K \in \mathcal{Q}_h^l(K)$, and $\hat{\mathbf{v}}_h \in \mathcal{M}_h^m$, where the bilinear forms are given by

$$\begin{aligned} a_{SMH}^E([\mathbf{u}_h, \hat{\mathbf{u}}_h], [\mathbf{v}_h, \hat{\mathbf{v}}_h]) &= 2\mu(\boldsymbol{\varepsilon}(\mathbf{u}_h), \boldsymbol{\varepsilon}(\mathbf{v}_h))_{\mathcal{T}_h} - 2\mu(\boldsymbol{\varepsilon}(\mathbf{u}_h) \mathbf{n}_K, (\mathbf{v}_h - \hat{\mathbf{v}}_h))_{\mathcal{E}_h} \\ &\quad + 2\mu\theta(\boldsymbol{\varepsilon}(\mathbf{v}_h) \mathbf{n}_K, (\mathbf{u}_h - \hat{\mathbf{u}}_h))_{\mathcal{E}_h} + \mathbf{s}_{SMH}([\mathbf{u}_h, \hat{\mathbf{u}}_h], [\mathbf{v}_h, \hat{\mathbf{v}}_h]), \end{aligned} \quad (12)$$

$$a_{SMH}^S(\phi_h, \varphi_h) = -\frac{1}{\lambda}(\phi_h, \varphi_h)_{\mathcal{T}_h}, \quad (13)$$

$$b_{SMH}(\phi_h, [\mathbf{v}_h, \hat{\mathbf{v}}_h]) = -(\phi_h, \operatorname{div} \mathbf{v}_h)_{\mathcal{T}_h} + \langle \phi_h, \pi_{\partial K}^m(\mathbf{v}_h - \hat{\mathbf{v}}_h) \cdot \mathbf{n}_K \rangle_{\mathcal{E}_h}, \quad (14)$$

$$f_{SMH}([\mathbf{v}_h, \hat{\mathbf{v}}_h]) = (\mathbf{f}, \mathbf{v}_h)_{\mathcal{T}_h}. \quad (15)$$

The stabilization bilinear form $s_{SMH}([\cdot, \cdot], [\cdot, \cdot])$ is very similar to that in the SPH formulation (9):

$$s_{SMH}([\mathbf{u}_h, \hat{\mathbf{u}}_h], [\mathbf{v}_h, \hat{\mathbf{v}}_h]) = 2\mu \frac{\beta_3}{h} \langle \pi_{\partial K}^m(\mathbf{u}_h - \hat{\mathbf{u}}_h), \pi_{\partial K}^m(\mathbf{v}_h - \hat{\mathbf{v}}_h) \rangle_{\partial \mathcal{T}_h},$$

where $\beta_3 > 0$ is a positive stabilization parameter crucial for obtaining coercivity.

5 Curved Meshes and Locking

The influence of choosing reference-frame polynomials to approximate unknowns defined over interfaces is that the polynomial order m for facets may have to increase as p , the effective mapping order¹ increases. This possible requirement is due to the fact that in all hybrid formulations presented before, one needs to compose physical-frame polynomials $\mathbf{v}_h|_e \in [\mathbb{P}_k^d(e)]^d$ for the interior with the mapping Ψ_e in order to integrate them over the boundary. Take, for example, integrals necessary to compute the $|J_{\Psi_e}|^{1/2}$ -weighted L^2 orthogonal projector π_σ^m of $v \in \mathbb{P}_k^d(e)$, with J_{Ψ_e} being the Jacobian of the mapping Ψ_e :

$$\int_\sigma (v \circ \Psi_e - \pi_\sigma^m)(\xi) w(\xi) |J_{\Psi_e}| d\xi = 0, \quad \forall w \in \mathbb{P}_m^{d-1}(\sigma).$$

Notice that we have, in this case, the inclusion $\mathbb{P}_k^d \circ \Psi_e \subseteq \mathbb{P}_{kp}^{d-1}$. As a result, in the view of the equation above, the approximation properties of the projection operator π_σ^m are determined by the largest value of k that satisfies $\mathbb{P}_k^d \circ \Psi_e \subseteq \mathbb{P}_m^{d-1}$. This discussion is presented in details in [18], in the context of HHO methods, where the authors show that assuming reasonable interpolation properties of $\pi_\sigma^m \circ \Psi_e$ leads to the following requirements to the polynomial order: $m = k - 1$ for $p = 1$, and $m = kp$ for $p > 1$. However, the authors also verified numerically that choosing $m = k$ when $p > 1$ seems to be enough for having an approximation order of $k + 1$ for the displacement in the interior. These results for HHO methods are all carried to the SPH and SMH formulations. It also turns out that this choice for the polynomial order k leads to locking-free methods on curved meshes, something that does not happen for the SPH formulation on straight meshes. These results are numerically verified in the next section.

6 Numerical Results

In this section we investigate the locking-free properties of the hybrid methods presented before, as well as their behavior in curved meshes. To effectively detect locking, we apply our formulation to solve a plane strain problem with $E = 1$, in which the solution for the displacement field is given by $u_1 = 2\nu \sin(\pi x) \cos(\pi y)$; $u_2 = (\nu - 1) \cos(\pi x) \sin(\pi y)$. Consequently, the solution to the hydrostatic pressure $\phi = -\lambda \operatorname{div} \mathbf{u}$ is given by $\phi = 2\nu\pi \cos(\pi x) \cos(\pi y)/(1 + \nu)$. Notice that even in the nearly incompressible limit $\nu \rightarrow 1/2$, the hydrostatic pressure is nonzero despite the fact that $\operatorname{div} \mathbf{u} \rightarrow 0$. The domain Ω in our tests is given by the unit square $[0, 1] \times [0, 1]$, and the Poisson modulus was chosen varying according to each case test. In all the experiments we use Dirichlet boundary conditions, given by the exact solution. For β_0 , β_1 and β_3 , we used the values described in [2]. We have only simulated symmetric formulations, which we obtain by choosing $\theta = -1$.

Figure 1 shows a sequence of triangular, trapezoidal and curved meshes. The trapezoidal meshes are obtained by distorting some nodes of a quadrangular mesh in the direction of the y -coordinate. The curved mesh is obtained by randomly altering the coordinates of 9-node elements in a square mesh.

Locking on straight meshes: the SMH and HHO methods have been proved to be uniformly stable in straight meshes (see [2] and [3]). However, the analysis for the SPH method has only been developed for the compressible case, as in [1]). Although the authors have also presented numerical evidence that the SPH formulation is locking-free when $\beta_1 = 0$ in [19], their analysis also suggests that both β_0 and β_1 need to be positive in order to obtain coercivity when $\theta \neq 1$. These are the results for the SPH method so far, when no projection is made to the boundary terms. We discuss now the influence of the projection operators on the locking-free property of the SPH formulation when $m = k - 1$. Figure 2 shows some results of h -convergence tests in triangular and trapezoidal meshes. We denote by $[\cdot]_{k,m}$ the $[\cdot]$ method with $\mathbb{P}_k^2(K)$, $K \in \mathcal{T}_h$, spaces in the interior and $\mathbb{P}_m^1(e)$, $e \in \mathcal{E}_h$, spaces at the boundary. We see that the lowest order combinations $\text{SPH}_{1,0}$, $\text{SMH}_{1,0}$ and $\text{HHO}_{1,0}$ are not stable in triangles, in general, as pictured by Fig. 2-(a), which is in accordance with other results in the literature. In trapezoids, however, the same combinations provide optimal L^2 convergence orders even with $\nu = 0.49999999$. On the other hand, $\text{SPH}_{1,1}$ optimally converges for triangles, while it does not have the same behavior for trapezoids, as pictured

¹Effective mapping order is understood as the minimal polynomial order necessary for the mapping. For example, for a 6-node triangle in $3d$, $p = 1$ or $p = 2$, while for a 9-node quadrilateral in $3d$, p can range from 4 to 1. When the mapping is affine, we have $p = 1$.

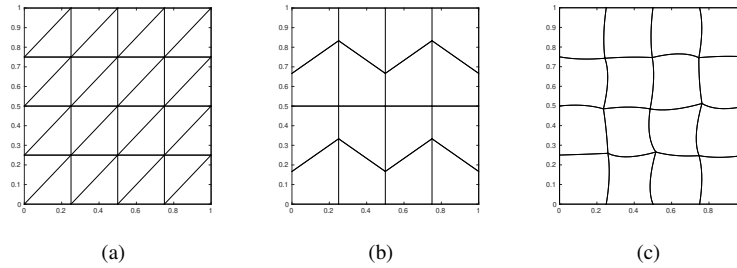


Figure 1. Meshes used in the simulations. Figure (a) shows a triangular mesh, figures (b) shows trapezoidal mesh and Figures (c) shows 9-node randomly distorted quadrilateral mesh with curved elements.

by Fig. 2-(a) and -(d). In general, the Fig. 2 suggests that all combinations $[\cdot]_{k,m}$ are locking free on triangles, for $m = k$ and $m = k - 1$, except in the lowest order $[\cdot]_{1,0}$. These results are expected for triangles, since the spaces $\mathbb{P}_k^2(K)$, $K \in \mathcal{T}_h$ are naturally divergence free (see BDM spaces in [20]). When K is a quadrilateral these spaces do not have the same property, and the optimal estimates in the incompressible limit have to be achieved by means of the formulation itself. This is the case of SMH and HHO methods, as shown in Fig. 2-(c), -(d) and -(e), where optimal convergence rates are observed in every combination. The analogous happens to the SPH method only if one chooses the combination $\text{SPH}_{k,k-1}$, which suggests that the projection operator at the boundary terms is *essential* for the optimal estimates. Among all these formulations, the SMH method is the most stable numerically: notice that the SPH and HHO methods may suffer from numerical issues that can drop convergence orders in the incompressible limit, as pictured in Fig. 2-(c). The SMH method also has the advantage of being less expensive than the HHO in its local problems, solved through the static condensation technique, though its local problems are slightly more expensive than those of the SPH method.

Locking on curved meshes: the convergence of the SPH, SMH and HHO methods on curved meshes has not been investigated before. The authors in [18] have a good discussion on this matter for the Poisson problem, however. Being a second order elliptic problem, we wondered whether their results would be valid also for the linear elasticity problem in the incompressible limit. Figure 3 shows an h -convergence test of the SPH, SMH and HHO methods on 9-node randomly distorted quadrilateral meshes. The first three figures, (a), (b) and (c) contain the convergence tests for the compressible case ($\nu = 0.3$), which allows us to identify when the method is unstable or not optimally convergent because of the spaces or formulation, and not locking. We notice that the combinations $[\cdot]_{k,k-1}$ are unstable on curved meshes, which agrees with the results of [18], since the *effective mapping order* is $p = 2$, in this case. The same figures also show that the combinations $[\cdot]_{k,k}$ are stable and optimally convergent, despite the apparent requirement that one would need $[\cdot]_{k,pk}$ in order to have such results. This is also in agreement with the conclusions in [18]. The following three figures, (d), (e) and (f), show the convergence order of the stable combinations in the near incompressible limit ($\nu = 0.49999999$). We notice that the locking-free property is maintained for the SMH and HHO methods. The combination $\text{SPH}_{k,k}$ also generates locking-free optimally convergent estimates for incompressible materials on 9-node randomly distorted quadrilaterals, although the same does not happen for 4-node trapezoids. The tests show that the convergence to the optimal order is slower, however, as figure (e) evidences. In this case we obtained the following sequence of convergence rates: 2.3, 2.5 and 2.9.

7 Conclusions

We have discussed the influence of projection operators on the boundary terms of two hybrid formulations for the linear elasticity problem, a primal and a mixed one, and the influence of these projections in the locking-free property of these formulations. We have also compared these methods with a hybrid high order method for the model problem. We have concluded that the cheapest method, the primal one, is uniformly stable in triangles, although compressible materials may cause rounding errors that influence numerical estimates in h -convergence tests. Similar behavior is encountered in the hybrid high order method, and the mixed hybrid method does not suffer from this problem. For quadrilaterals, the primal method is only stable if one uses approximation spaces one order smaller for the Lagrange multipliers, in comparison with the order of the displacement field. The other methods are locking-free on quadrilaterals independent of this restriction. Finally, we observed that all methods are unstable if one chooses smaller approximation spaces for Lagrange multipliers on a 9-node randomly distorted quadrilateral mesh. It suffices to have same order approximation spaces for interior and boundary in this type of mesh, for all methods, which are also locking-free in this scenario.

We are currently devising proofs for the results observed numerically, which will be presented in a future

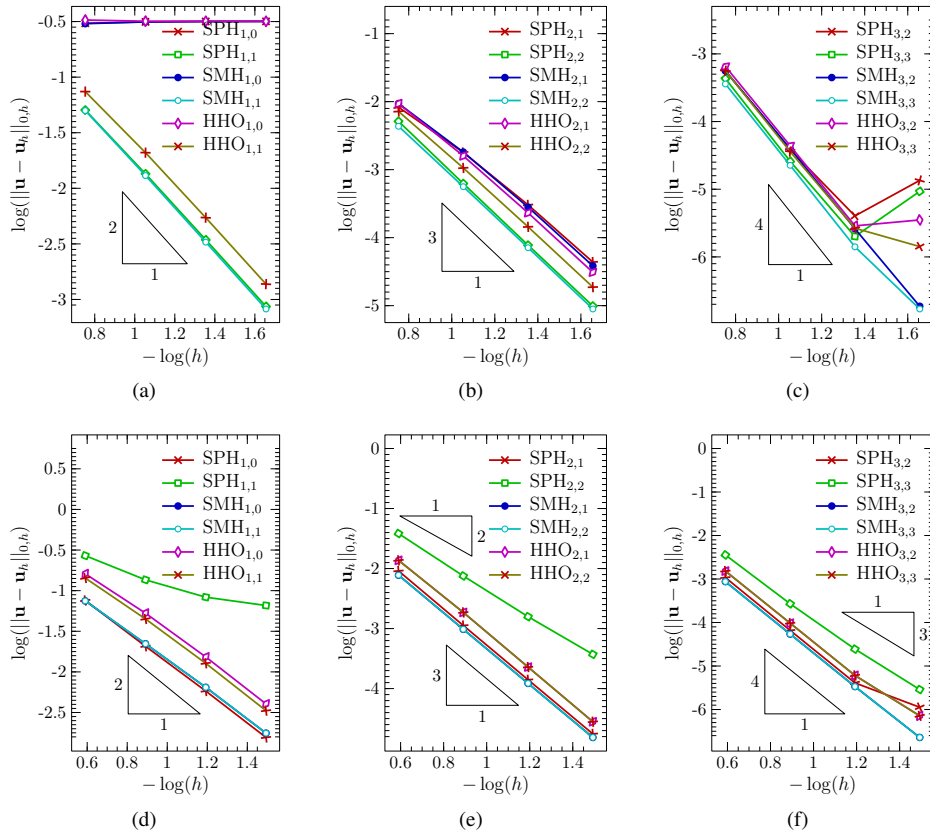


Figure 2. h -convergence tests for triangular ((a), (b) and (c)) and trapezoidal ((d), (e) and (f)) meshes, as in Figure 1 ($\nu = 0.49999999$).

work. The locking-free property for the primal hybrid formulation is built from the results in [21] and [15], but the results for curved meshes remain without proofs in the literature.

The authors hereby confirm that they are the sole liable persons responsible for the authorship of this work, and that all material that has been herein included as part of the present paper is either the property (and authorship) of the authors, or has the permission of the owners to be included here.

References

- [1] Faria, C. O., Loula, A. F., & dos Santos, A. J., 2014. Primal stabilized hybrid and DG finite element methods for the linear elasticity problem. *Computers & Mathematics with Applications*, vol. 68, n. 4, pp. 486 – 507.
- [2] Ledoino, I. S., 2018. Hybrid DG Methods for Biot's Consolidation Problem. Master's thesis, Laboratório Nacional de Computação Científica - LNCC, Petropolis - RJ, Brazil.
- [3] Di Pietro, Daniele A.; Ern, A., 2015. A hybrid high-order locking-free method for linear elasticity on general meshes. *Computer Methods in Applied Mechanics and Engineering*, vol. 283.
- [4] Arnold, D. N., Brezzi, F., & Douglas Jr., J., 1984. PEERS: A new mixed finite element for plane elasticity. *Japan Journal of Applied Mathematics*, vol. 1, n. 2, pp. 347–367.
- [5] Franca, L. P., Hughes, T. J. R., Loula, A. F. D., & Miranda, I., 1988. A new family of stable elements for nearly incompressible elasticity based on a mixed Petrov-Galerkin finite element formulation. *Numerische Mathematik*, vol. 53, pp. 123–141.
- [6] Arnold, D. N. & Winther, R., 2002. Mixed finite elements for elasticity. *Numerische Mathematik*, vol. 92, n. 3, pp. 401–419.
- [7] Adams, S. & Cockburn, B., 2005. A mixed finite element method for elasticity in three dimensions. *Journal of Scientific Computing*, vol. 25, n. 3, pp. 515–521.
- [8] Awanou, G., 2013. Rectangular mixed elements for elasticity with weakly imposed symmetry condition. *Advances in Computational Mathematics*, vol. 38, n. 2, pp. 351–367.
- [9] Ciarlet, P. G., 1978. *The Finite Element Method for Elliptic Problems*. SIAM.

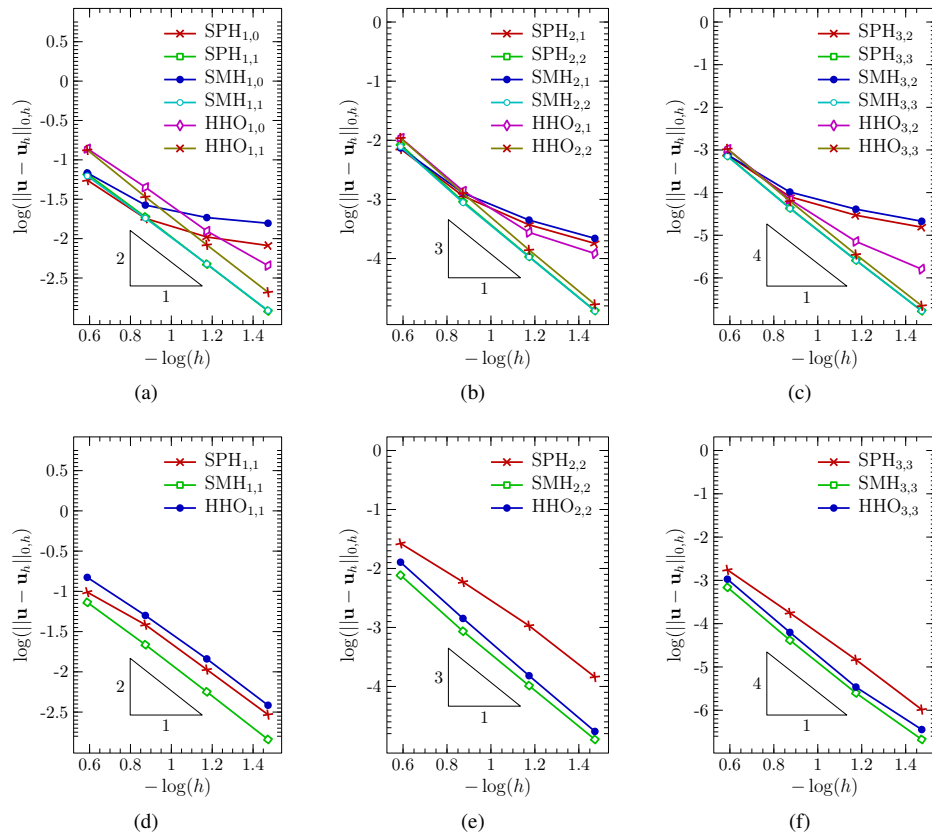


Figure 3. h -convergence tests for 9-node randomly distorted meshes, as in Figure 1. The compressible case is considered in figures (a), (b) and (c) ($\nu = 0.3$), while the incompressible case is considered in figures (d), (e) and (f) ($\nu = 0.49999999$).

- [10] Arnold, D. N., Falk, R. S., & Winther, R., 2007. Mixed finite element methods for linear elasticity with weakly imposed symmetry. *Mathematics of Computation*, vol. 76, n. 260, pp. 1699–1723.
- [11] Qiu, W. & Demkowicz, L., 2009. Mixed hp-finite element method for linear elasticity with weakly imposed symmetry. *Computer Methods in Applied Mechanics and Engineering*, vol. 198, n. 47–48, pp. 3682–3701.
- [12] Quinelato, T. O., 2017. *Mixed hybrid finite element method in elasticity and poroelasticity*. PhD thesis, Laboratório Nacional de Computação Científica - LNCC, Petrópolis-RJ, Brazil.
- [13] Rivière, B. & Wheeler, M. F., 2000. Optimal error estimates for discontinuous Galerkin methods applied to linear elasticity problems. *Comput. Math. Appl.*, vol. 46, pp. 141–163.
- [14] Wihler, T. P., 2006. Locking-free adaptive discontinuous Galerkin FEM for linear elasticity problems. *Mathematics of Computation*, vol. 75, n. 255, pp. 1087–1102.
- [15] Hansbo, P. & Larson, M. G., 2002. Discontinuous Galerkin methods for incompressible and nearly incompressible elasticity by Nitsche’s method. *Comput. Methods Appl. Mech. Engrg.*, vol. 191, n. 17–18, pp. 1895–1908.
- [16] Cockburn, B., Schötzau, D., & Wang, J., 2006. Discontinuous Galerkin methods for incompressible elastic materials. *Comput. Methods Appl. Mech. Engrg.*, vol. 195, pp. 3184–3204.
- [17] Babuška, I., 1971. Error bounds for finite element method. *Numerische Mathematik*, vol. 16, pp. 322–333.
- [18] Botti, L. & Di Pietro, D. A., 2018. Assessment of hybrid high-order methods on curved meshes and comparison with discontinuous galerkin methods. *Journal of Computational Physics*, vol. 370, pp. 58 – 84.
- [19] SANTOS, A. D., FARIA, C., & LOULA, A., 2017. A Stabilized Hybrid Discontinuous Galerkin Method for Nearly Incompressible Linear Elasticity Problem. *TEMA (SÃO Carlos)*, vol. 18, pp. 467 – 477.
- [20] Brezzi, F. & Fortin, M., 1991. *Mixed and Hybrid Finite Element Methods*. Springer-Verlag.
- [21] Oikawa, I., 2015. A hybridized discontinuous Galerkin method with reduced stabilization. *Journal of Scientific Computing*, vol. 65, n. 1, pp. 327–340.